AGU PUBLICATIONS

JGR

Journal of Geophysical Research: Solid Earth

RESEARCH ARTICLE
10.1002/2013JB010351

Key Points:
- Groundwater discharge is not significantly higher or lower for inactive faults
- Groundwater discharge is significantly higher in orogen than crystalline bedrock
- New method uses groundwater discharge to examine regional permeability of faults

Supporting Information:
- Readme
- MalgrangeSM 15Dec

Correspondence to:
Tom Gleeson,
tom.gleeson@mcgill.ca

Citation:
Malgrange, J., and T. Gleeson (2014), Shallow, old, and hydrologically insignificant fault zones in the Appalachian orogen, *J. Geophys. Res. Solid Earth*, *119*, 346–359, doi:10.1002/2013JB010351.

Received 14 MAY 2013
Accepted 30 DEC 2013
Accepted article online 4 JAN 2014
Published online 29 JAN 2014

Shallow, old, and hydrologically insignificant fault zones in the Appalachian orogen

Juliette Malgrange[1] and Tom Gleeson[1]

[1]Civil Engineering and Applied Mechanics, McGill University, Montréal, Quebec, Canada

Abstract The permeability of fault zones impacts diverse geological processes such as hydrocarbon migration, hydrothermal fluid circulation, and regional groundwater flow, yet how fault zones affect groundwater flow at a regional scale (1–10 km) is highly uncertain. The objective of this work is to determine whether faults affect regional patterns of groundwater flow, by using radioactive radon and chloride to quantify groundwater discharge to lakes underlain by faults and not underlain by faults. We sampled lakes overlying the Paleozoic Appalachian fold and thrust belt in the Eastern Townships in Québec, and compared our results to a previous study in a crystalline watershed in the Canadian Shield. The field data was analyzed with an analytical geochemical mixing model. The uncertainties of model parameters were assessed in a sensitivity analysis using Monte Carlo simulation, and the difference between lakes tested with statistical analysis. While the model results indicate non-negligible groundwater discharge for most of the lakes in the Paleozoic orogen, the difference between the groundwater discharge rate into the lakes located on faults and the other lakes is not statistically significant. However, the groundwater discharge rate to lakes in the Paleozoic orogeny is significantly higher than lakes that overlay crystalline bedrock, which is consistent with independent estimates of permeability. The rate of groundwater discharge is not significantly enhanced or diminished around the thrust fault zones, suggesting that in a regional scale, permeability of fault zones is not significantly different from the bedrock permeability at shallow depth in this old, tectonically- inactive orogen.

1. Introduction

The permeability of fault zones is complex, heterogeneous, and difficult to predict a priori or without detailed study. Depending on the type, age, lithology, geometry, and geologic history of the fault zone, they may act as conduits, barriers, or combined conduit-barrier systems that enhance or impede fluid flow [*Aydin*, 2000; *Caine et al*., 1996; *Childs et al*., 2009; *Faulkner et al*., 2010]. At a local scale fault zones are often described as composed of two distinct components: a fault core, a zone of high strain where most of the displacement is accommodated, and flanked by a damage zone of lesser strain, that is mechanically related to the growth of the fault zone [*Caine et al*., 1996; *Chester and Logan*, 1986; *Evans et al*., 1997]. Fault zone permeability has been studied extensively at a local scale (1–100 m) but very few field-based studies focus on how faults impact regional scale (1–10 km) groundwater flow. Hydrogeological studies have successfully observed and modeled the rate and/or direction of fluid flow around fault zones at local scales [*Bense et al*., 2013; *Bense and Person*, 2006; *Bense et al*., 2008; *Fairley et al*., 2003; *Fairley and Hinds*, 2004; *Leray et al*., 2013, 2012; *Seaton and Burbey*, 2005]. Testing fault permeability models with subsurface hydrogeological data is often hampered by a limited understanding of three-dimensional fluid flow patterns and processes driving fluid flow which is crucial [*Bense et al*., 2013]. Although the effect of fault zones on local groundwater flow can be significant, we investigate whether fault zones systematically affect regional groundwater flow significantly. We estimate groundwater discharge in order to characterize how fault zones affect permeability at a regional scale.

Groundwater flow into any water body, called groundwater discharge, can be characterized through a number of methods using environmental tracers such as temperature, stable isotopes, or dissolved gases [*Hayashi and Rosenberry*, 2002; *Kalbus et al*., 2006; *Sophocleous*, 2002]. Naturally occurring radon (^{222}Rn) has been widely used to quantify groundwater discharge to rivers [*Cook*, 2003; *Cook et al*., 2006], wetlands [*Cook et al*., 2008], lakes [*Dimova et al*., 2013; *Gleeson et al*., 2009; *Kluge et al*., 2007, 2012], or oceans [*Taniguchi et al*., 2002]. Radon-222 (^{222}Rn) is a radioactive noble gas produced by natural decay of radium-226 (^{226}Ra), which is

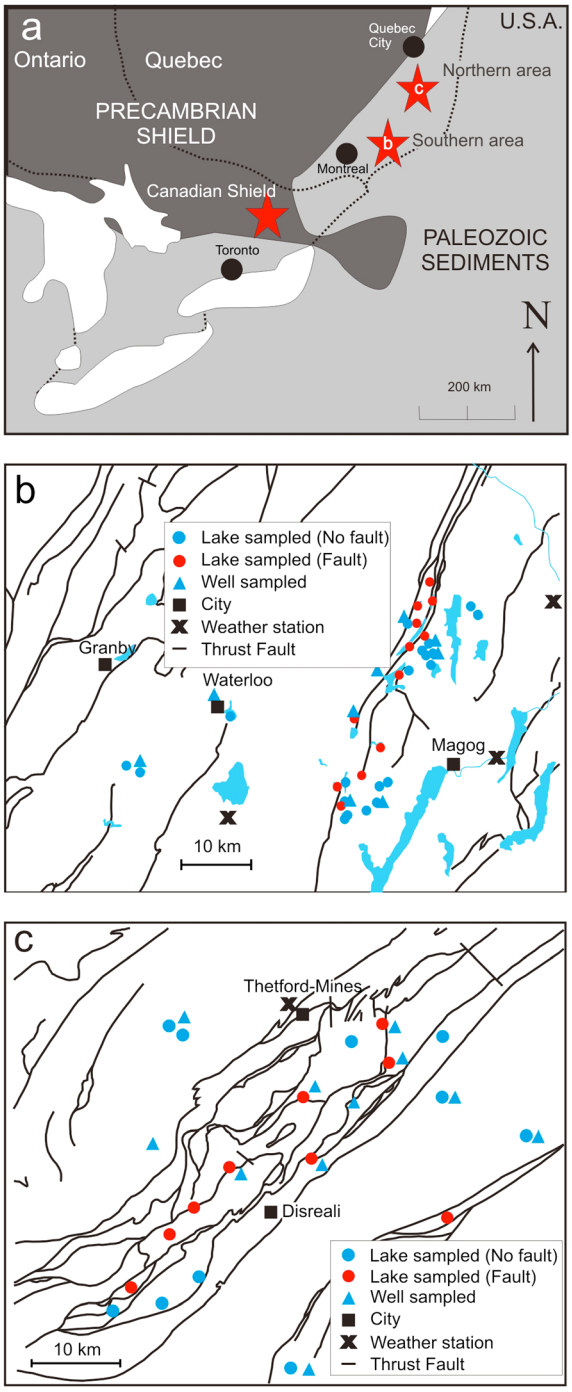

Figure 1. (a) Study area. The sampling area was divided into two zones: the (b) southern area, with 34 lakes sampled, and the (c) northern area, with 20 lakes sampled. The third area shown in Figure 1a is the region of *Gleeson* [2009] study in the Canadian Shield.

part of the natural decay chain of uranium-238 (^{238}U). Due to the large difference in activities between groundwater and surface water, its nonreactivity and its rapid decay, radon is a powerful, efficient, and accurate groundwater tracer. Although groundwater discharge has been studied qualitatively in fractured bedrock aquifers [*Oxtobee and Novakowski*, 2002; *Praamsma et al.*, 2009], methods developed in the field of groundwater-surface water interactions have not been applied to fluid flow around faults.

The objective of this study is to assess whether tectonically inactive fault zones impact the groundwater discharge rates to overlying lakes. Groundwater discharge was quantified for 54 lakes in Eastern Quebec,

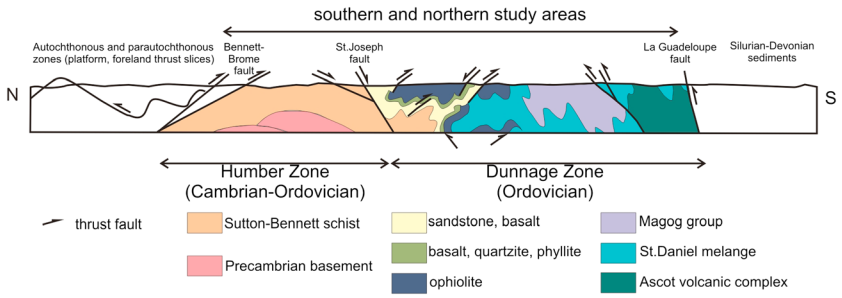

Figure 2. Schematic, composite structural cross section through the northern and southern study areas in southern Quebec (~100 km long, ~5 km depth). The Humber and Dunnage zones of the Appalachian orogen, shown in color are the focus of sampling. Adapted from *Schroetter et al*. [2006].

using a mixing model of natural-occurring tracers, radon (^{222}Rn) and chloride. We sampled 21 lakes overlying thrust faults in the Appalachian Mountains in the Eastern Townships and Chaudière-Appalaches, east of Montréal, Québec as well as 33 lakes not underlain by a fault zone within the same region (Figure 1). We also compared results to similar results computed by *Gleeson et al*. [2009] who used the same methodology to estimate groundwater discharge rates to lakes underlain by crystalline rock in the Canadian Shield. Darcy's law indicates that differences in groundwater discharge are due to differences in hydraulic gradient or permeability. In these humid regions the water table is generally near the surface [*Winter*, 1999; *Winter et al*., 1998], and the topographic gradients are generally consistent, suggesting that differences in groundwater discharge would most likely be due to differences in permeability. Therefore, by comparing groundwater discharge to lakes located on a fault zone and to lakes away from any fault zone, we can assess whether fault zones significantly affect the regional subsurface hydrology due to their difference in permeability relative to the surrounding bedrock. The uncertainty of the model due to measurements errors or inaccuracy in parameters estimations was investigated using Monte Carlo simulations.

2. Field Areas

Three study areas are shown in Figure 1. Our present study was carried out in the first two areas, located in the Appalachian orogen in southern Québec, Canada in September to November 2011. The southern area (Figure 1b) is located around Magog, about 100 km east of Montreal, in the Eastern Townships. The northern area (Figure 1c) is located around Thetford-Mines, about 100 km south of Québec City, in the region of Chaudière-Appalaches. The third area shown in Figure 1a corresponds to the study carried out by *Gleeson et al*. [2009] in the Canadian Shield that we use as a comparison for our results. It is located in rural eastern Ontario, Canada, in the ~900 km^2 Tay River watershed. The hydrology, climatology, and geology of the third area are described by *Gleeson et al*. [2009].

Four tectonostratigraphic zones are recognized in southern Quebec, from northwest to southeast: the (1) Grenville Province, (2) the St. Lawrence platform, (3) Appalachian foreland basin (autochthonous domain), a fault-imbricated zone (parautochthonous domain), and (4) the Appalachian thrust sheets (allochthonous domain) [*De Souza and Tremblay*, 2010; *Sasseville et al*., 2008; *Schoonmaker and Kidd*, 2007; *Schroetter et al*., 2005, 2006; *Séjourné et al*., 2003; *Séjourné and Malo*, 2007; *Séjourné et al*., 2005]. The southern and northern study areas are located in the Appalachian thrust sheets (Figure 2) which are generally divided into the Cambrian-Ordovician Humber and Dunnage Zones [*Schroetter et al*., 2006; *Williams*, 1979]. The Humber Zone consists of a series of low-grade sedimentary and volcanic rocks such as shales and, phyllites deformed by a series of northwest directed thrusts. The most extensive geological unit underlying the sampled lakes is the phyllitic Sutton-Bennett schist [*St-Julien and Slivitzsky*, 1985]. The Dunnage Zone is an Ordovician oceanic domain of ophiolites, mélanges, volcanic arc sequences, and marine flysch deposits obducted during the Taconian orogeny. The most extensive geological units underlying the sampled lakes are an ophiolitic sequence comprised of serpentinite, pyroxenite, and volcanics [*St-Julien and Slivitzsky*, 1985]. The thrust slices are locally intruded by a Cretaceous gabbro.

The faults are primarily thrust faults, including some back thrusts [*Schroetter et al*., 2005, 2006]. Fault deformation occurred before, during, and after the Ordovician Taconian orogeny, during the Late Silurian to early

Devonian and during the Devonian Acadian orogeny [*Sasseville et al*., 2008; *Séjourné and Malo*, 2007]. Therefore, some of the fault deformation is of similar age to the deformed lithologies. Some faults are named (Figure 2) but most are not (see distribution of faults in Figures 1b and 1c).

The lakes we sampled in the southern and northern study areas are mainly small lakes with areas ranging from 0.05 to 4 km^2 and depths ranging from 0.3 to 35 m. We sampled 34 lakes in the southern area, within a radius of 30 km, and 20 lakes in the northern area also within a radius of 30 km. Few streams typically enter the lakes, some of the lakes having no discernible or mapped inlet. Some lakes are independent without nearby lakes in their watershed, whereas other lakes are part of small interconnected lake systems. The water temperature of our samples ranged from 5°C to 20°C.

Both regions in Québec have undulating valley and ridge topography with gentle relief with up to 800 m of elevation. There are very few agricultural activities, and the land is mainly covered with deciduous forest dominated by sugar maples, yellow birches, beeches, and red oaks. The climate is humid and continental, with daily temperatures annually ranging from −16°C to 25°C. The average air temperature during our sampling was ~10°C. The annual precipitation ranges between 900 and 1000 mm, and the annual snowfall is between 200 and 400 cm. The average precipitation is ~100 mm, 90 mm, and 70 mm respectively in September, October, and November.

3. Methods

3.1. Field Sampling and Laboratory Analysis

Gleeson et al. [2009] developed a steady state advective model using radon (^{222}Rn) and chloride budgets for quantifying groundwater discharge rate, schematized in Figure 3, which is expressed as follows:

$$\frac{\partial v}{\partial t} = I_s + I_g + P \cdot A - E \cdot A - Q = 0 \tag{1}$$

where the combined groundwater and surface water outflow Q can then be expressed as a function of I_s, the surface water inflow rate (m^3/day), I_g the groundwater inflow rate (m^3/d), P the precipitation rate (m/d), A the surface water area (m^2), and E the evaporation rate (m/d).

For the chloride, the inflow from surface water, groundwater, and precipitation are balanced with the outflow Q, leading to the following equation:

$$C_{Cl} \cdot Q = I_S \cdot C_{s,Cl} + I_g \cdot C_{g,Cl} + P \cdot A \cdot C_{p,Cl} \tag{2}$$

where C_{Cl} is the chloride concentration in the lake, $C_{s,Cl}$ is the chloride concentration in the incoming surface water, $C_{g,Cl}$ is the chloride concentration in the groundwater, and $C_{p,Cl}$ is the chloride concentration in precipitation.

For the radon, which is assumed negligible in precipitation, the inflow from surface and groundwater is balanced with the outflow, the radioactive decay, and the gas exchange as describes the equation:

$$C_{Rn} \cdot (Q - k \cdot A + \lambda \cdot V) = I_s \cdot S_{s,Rn} + I_g \cdot C_{g,Rn} \tag{3}$$

where λ is the radioactive decay constant (day^{-1}), V the volume of the lake (m^3), k the gas exchange velocity (m/d), C_{Rn} is the radon activity in the lake, $C_{s,Rn}$ is the radon activity in the incoming surface water, and $C_{g,Rn}$ is the radon activity in the groundwater. We assume indeed that both the diffusive radon flux from the lake sediments and radon produced by radium decay are negligible. Radium activity in water is indeed low, since radium is a bound on sediment particles in fresh water [*Kiro et al*., 2012], and its half-life of about 1600 years makes radon production from radium decay negligible. Radon diffusive flux in lakes has been studied by *Cook et al*. [2008] and is further discussed in

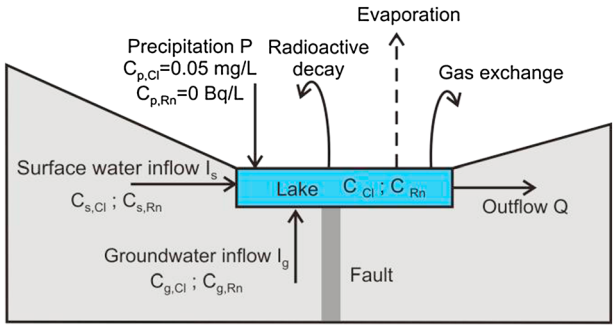

Figure 3. Schematic of the steady state model. Variable names are defined in the text.

the supporting information. For the lakes with low groundwater discharge, the radon diffusive flux can become important, and in these cases, the discharge rate calculated may be overestimated. This is a one-box model for each lake, whereas a more precise, multibox model has recently been developed for a detailed study of a single lake [*Kluge et al*., 2012]. Results of one-box models can be consistent with multibox models if a representative radon concentration is used [*Kluge et al*., 2012].

Equations (1)–(3) were simultaneously solved for each lake to determine the three unknown factors I_g, I_s, and Q. For the lakes with no major inlets—19 lakes are concerned—the discharge rate is calculated taking $I_s = 0$.

The radioactive decay constant for radon is $\lambda = 0.18\ \text{day}^{-1}$. *Cook et al*. [2008] estimated the gas exchange velocity for radon k from measurements of the gas transfer rate between wetland and the atmosphere of an injected tracer, SF_6, carried out in Australia. The measurements lead to a gas transfer velocity of $k = 0.16$ m/d, which is the value we adopted. The steady state model is not very sensitive to the gas transfer velocity since the lakes are relatively deep [*Cook et al*., 2008]. Moreover, the emphasis of our study is to assess the difference between lakes and so an error on the gas exchange rate will shift all our results and will not change our conclusion.

Field work was conducted during low-flow conditions in the late summer and early fall 2011. Lakes were sampled from either private docks, boats, or directly from the shore for both chloride (C_{Cl}) and radon (C_{Rn}) analysis. Water was sampled about 10 to 20 cm under the surface in order to minimize air contamination, and during the late summer and early fall likely after the turnover of summer stratification so that radon activities would be well mixed. If still stratified, these shallow samples are from within the epilimnion which can have a radon activity corresponding approximately to the lake average [*Kluge et al*., 2007] or lower [*Kluge et al*., 2012]. Inflowing chloride concentrations ($C_{S,Cl}$) and radon activities ($C_{S,Rn}$) were determined by sampling all major inlets during low-flow conditions to ensure representative concentrations. When more than one stream was discharging to the lake, the inflowing chloride concentration and radon activity was estimated by a stream flow-weighted mean. Stream flow was measured with a propeller with a precision of 0.1 m/s, estimating the flow of 5 to 10 points on a transection of the stream, where the water was sampled.

Groundwater samples were collected from 20 private wells across our study area (Figures 1b and 1c). The depths of wells range from 20 to 100 m below ground surface. The water was collected mainly from outside taps, ensuring that the water was unfiltered. Since the groundwater radon activity varies widely even over short distances, we were not able to accurately estimate the radon activity in groundwater that discharges to each lake. Instead, we use the mean value for $C_{g,Rn}$ for all the lakes and assess the uncertainty due to the natural variability of radon activities, as described below. Similarly, we use the mean value for chloride concentration in groundwater $C_{g,Cl}$.

Radioactivity of radon was measured using the liquid scintillation counter *Hidex 300 SL* with a detection limit of 0.01 Bq/L and chloride concentrations using ion chromatography, with a detection limit of 0.1 mg/L.

Lake area, watershed area, and topographic gradients were derived in ArcGIS from Geobase Canada and *DMTI* [2010]. Lake depths were derived from a report by *Prairie and Soucisse* [1999] or from field measurements and estimates. Lake volume (V) was estimated from the area and depth of each lake. The precipitation rate (P) was assessed, from the daily values at four meteorological stations in the Eastern Townships and Chaudière-Appalaches: Magog (45°16′N; 72°07′E), Brome (45°11′N; 72°34′E), Bromptonville (45°29′N; 71°57′E), and Thetford-Mines (46°06′N; 71°21′E). An average over the week preceding the sampling was computed for each lake, using the station in Thetford-Mines for the lakes within the northern region, and an average on the three other stations for the lakes in the southern region. Chloride concentration in precipitation ($C_{P,Cl}$) was extracted from the *Canadian National Atmospheric Chemistry database*, at the station in Frehligsburg (45°03′N; 72°51′E), about 50 km southwest of the southern study area. Radon activity in precipitation is assumed to be negligible.

3.2. Sensitivity and Statistical Analysis

The model sensitivity to parameter uncertainty was assessed first by observing the variations of the discharge rates as a function of each parameter for a "typical" lake, whose parameters are taken as the average value of the values of the 54 lakes. Additionally, we varied every parameter individually by ±20% and by ±50% and averaged the changes in groundwater discharge rates for each lake in each case. The robustness of the results given the parameter uncertainty was also investigated using a Monte Carlo approach. First, we calculated the uncertainty in discharge rates due to uncertainty in the radon activity in groundwater, which has a high heterogeneity and sensitivity. We ran the steady state model for each lake 5000 times, varying only the radon activity in groundwater, assuming a lognormal distribution with the mean and the standard deviation of the

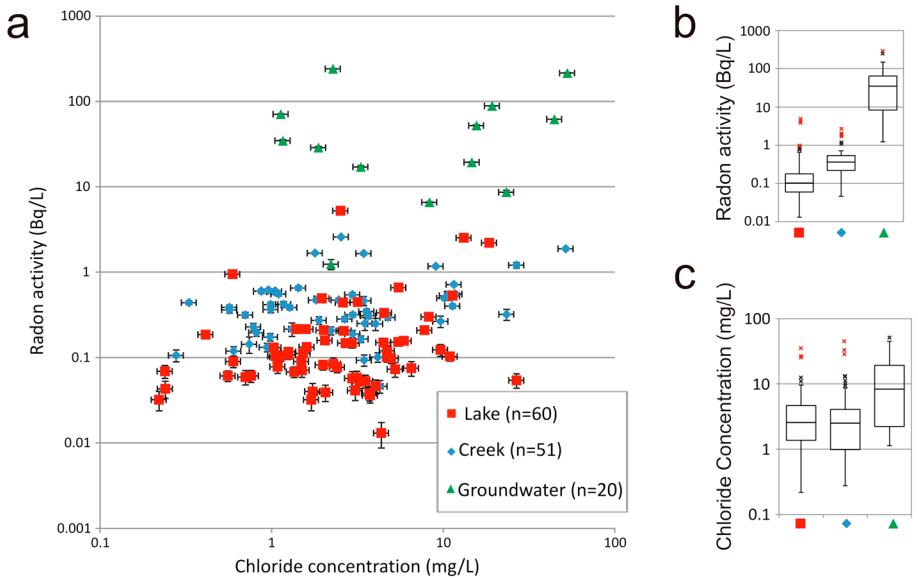

Figure 4. (a) Radon activity and chloride concentration for the three types of water bodies sampled: lakes, creeks, and groundwater. The error bars are measurement errors and do not account for the potential uncertainty due to sampling location and time. (b and c) The boxplot representing the distribution of respectively radon activities and chloride concentrations in the data. The boxes include 50% of the samples, from the first quartile (Q1) to the third quartile (Q3). The negative error bar indicates the minimum observed value, and the positive error corresponds to one and a half interquartile range. The outliers are shown with a black cross, whereas extreme outliers (the points that exceed the third quartile by more than three interquartile ranges) are shown by a red cross. Each lake sample is shown, and some lakes were sampled twice to ensure reproducibility so the number of lake samples is greater than the number of lakes.

20 groundwater samples. Then we assessed the cumulative uncertainty of all models parameters (lake area, lake depth, radon activity in lake, inflow and groundwater, chloride concentration in lake, inflow, groundwater and precipitation, and precipitation and evaporation rates) on the calculated discharge rate to each lake. This analysis also calculated the discharge rate for 5000 simulations for each lake, while varying all variables simultaneously, assuming the uncertainties follow a normal distribution with a mean equal to the previously estimated value, and a standard deviation equal to 20% of the mean, ensuring the actual values of all variables be within 60% of the estimated values with 95% probability.

The groundwater discharge rates to lakes overlying faults and other lakes were compared using two statistical tests for distinguishing two populations: the Welch's *t* test and the Kolmogorov-Smirnoff's test [*Lilliefors*, 1967; *Marsaglia et al.*, 2003; *Massey*, 1951; *Miller*, 1956]. The Welch's method tests the null hypothesis stipulating that the means of both data sets are equal, whereas the Kolmogorov-Smirnoff's method tests the null hypothesis stipulating that both data sets are from the same continuous distributions. Additional description of the statistical methods is found in the supporting information. Herein a value is considered an outlier if it plots above the positive error bar, defined as one and a half interquartile range on the boxplot or an extreme outlier if the value exceeds the third quartile by more than three interquartile ranges. We also computed both tests for each of the 5000 Monte Carlo simulations, and we estimated the frequency of rejecting the null hypothesis suggesting that groundwater discharge rates are the same in presence of a fault zone. Both statistical tests were also run to compare the simulated data with the data from the Canadian Shield, also treated with a Monte Carlo simulation for the uncertainty of radon activity in groundwater.

4. Results and Discussion

4.1. Field Sampling and Laboratory Analysis

Radon and chloride activities of all the water bodies sampled are shown in Figure 4. The mean radon activity in groundwater (54 Bq/L) is 2 orders of magnitude higher than in surface water (0.5 Bq/L for creeks and 0.3 Bq/L for lakes) which confirms the validity of radon as groundwater tracer. The distribution of radon activity in the lakes is relatively well distributed with five extreme outliers with radon activities of 5.2 Bq/L, 2.5 Bq/L, 2.2 Bq/L, 0.9 Bq/L, and 0.7 Bq/L (Figure 4b). The remaining lakes have an average radon activity of 0.15 Bq/L, with a standard deviation of 0.12 Bq/L. The mean radon content in lakes, with an average of 0.32 Bq/L, is high in the combined

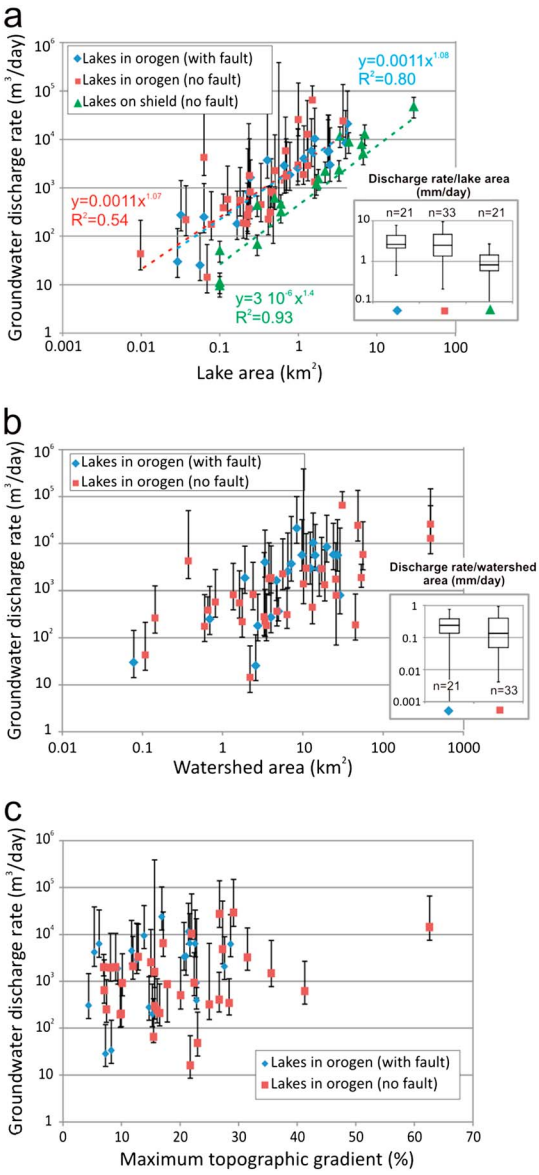

Figure 5. The groundwater discharge rates estimated through the steady state model are plotted for the two categories of lakes (fault or no fault) versus (a) the lake area, (b) the watershed area, and (c) the maximum topographic gradient. Data from *Gleeson* [2009] are also represented in the first graph (lakes on shield). The orogen is an Appalachian orogen, composed of metamorphosed volcanic and sedimentary rocks, whereas the shield refers to the Canadian Shield composed of crystalline rocks. The distribution of the ratio of the groundwater discharge rates to the lakes areas in Figure 5a and to the watershed areas in Figure 5b are also represented with a boxplot.

northern and southern area, as compared to the Canadian Shield where the average activity of radon in the lakes was about 0.009 Bq/L [*Gleeson*, 2009].

Radon activity in groundwater is relatively heterogeneous, and the standard deviation (65 Bq/L) is higher than the mean (54 Bq/L) if all samples are included. Figure S1b in the supporting information shows the radon activity measured in the wells in the southern area (Magog and Bromont), in the northern area (Disraeli), as well as the values measured by Gleeson et al. in the Canadian Shield. The two wells sampled in the Bromont area show a much higher radon activity than the other wells, respectively 240 Bq/L and 214 Bq/L, whereas the average radon activity in groundwater is 30 ± 5 Bq/L and 40 ± 5Bq/L in respectively the southern and the northern area. The two regions with high radon activity correspond to a gabbro intrusion (see Figure S1c) with magmatic rocks which likely explains the high radon activity. Hence, we assigned the three lakes (Waterloo, Bromont, and Gale) in the Bromont region a different value for the radon activity in groundwater, equal to the average of both samples (227 Bq/L). Then, we assigned the same value for the other lakes of both regions, equal to the averaged estimation of all samples but the two former, which is then 34.5, with a standard deviation of 28.8 Bq/L. Since radon activity in groundwater highly varies spatially even around a single lake, and since the sample sizes of groundwater for both areas are too small to enable an accurate estimate of the actual value of radon in groundwater, the value assigned to all lakes seems to be the best estimate, although the observed means differ in southern and northern areas. Like other field areas, the radon activity in groundwater is relatively uncertain due to the variable production and transport of uranium [*Folger et al.*, 1996]. Therefore, we consider our average value a reasonable estimation of the average groundwater that discharges to the lakes in the study area.

Chloride concentrations have overlapping concentrations for the different types of water bodies: in groundwater (13.8 ±18 mg/L), creeks (5 ± 8.5 mg/L), and lakes (4.1 ± 4.8 mg/L). As opposed to radon, chloride does not show any geographical pattern.

4.2. Steady State Model

Using the steady state model, we estimated the groundwater discharge rate to each of the 54 lakes. The groundwater discharge rates are plotted in Figure 5 against three topographic and geometric parameters that control groundwater flow: the lake area, the watershed area, and the maximum topographic gradient, which is used as a proxy for the mean topographic gradient.

In Figure 5a, we plotted the calculated discharge rates for each lake against their areas, for both groups of lakes in the Appalachian orogen (the ones located on a fault and the ones located away from a fault), as well

as for the lakes from the Canadian Shield that do not overlie a fault. As expected, the total discharge rate increases with lake area, which supports the overall validity of the analytical model. Also, the lakes from the Canadian Shield generally have smaller discharge rates than the lakes in the Appalachian orogen for a given lake area. The median area-averaged flux (groundwater discharge rate normalized by the lake area) for lakes in the Appalachian orogen located on a fault (2.4 mm/d) is very similar to the median discharge rate for lakes that are not underlain a fault zone (2.3 mm/d). The median area-average discharge rate for lakes in the Canadian Shield is much lower (0.9 mm/d), suggesting that the groundwater discharge is more significant in the metamorphosed sedimentary and volcanic rocks of the Appalachians than in the crystalline bedrock. The distributions of the discharge rates to lakes in the Appalachian orogeny underlain by a fault and to the others without fault are similar, and the two data sets cannot be differentiated on the boxplot (Figure 5a), except that the discharge rates to lakes which are not underlain by a fault zone are more broadly distributed. The high variability of the groundwater discharge rates in our field study, with discharge rates ranging from 0.2 mm/d to 68 mm/d could be explained by the differences in watershed characteristics, aquifer permeability, and local geography or aquifer geometry.

The groundwater discharge rate also depends on the recharge flux that occurred upstream, which can be approximated by the watershed area. Figure 5b represents the estimated discharge rates of the 54 lakes in the Appalachians plotted versus their watershed areas, estimated with ArcGIS. The groundwater discharge rate also increases with watershed area. The inset boxplot shows the distribution of the groundwater discharge rates normalized by the watershed area for both lakes underlying a fault zone and lakes that are not located on a fault zone. Again, the distributions of both data sets are very similar, except that the data are more broadly distributed for the lakes not underlain a fault. The median ratio of the discharge rates to the watershed areas is 0.24 mm/d for the lakes underlying a fault and 0.14 mm/d for the other lakes. And 50% of the data are between 0.14 and 0.4 mm/d for the lakes located on a fault and between 0.05 and 0.4 mm/d for the other lakes. Hence, after normalizing the discharge rates to the associated watershed areas, there is still no discernible difference between the lakes located on a fault zone and the other lakes.

Although hydraulic gradients drive groundwater flow, there is no obvious correlation between maximum topographic gradient in a watershed and groundwater discharge rate (Figure 5c). Therefore, although we cannot exclude the fact that topography can control the groundwater discharge rate, topography does not explain the major differences between the calculated values of discharge rate. Furthermore, again there is no difference noticeable between the lakes located on fault and the lakes not underlain by a fault.

For all the further analysis, we average groundwater discharge rates over the lake area for two reasons. First, this area-averaged flux is effectively the Darcy flux which is proportional to the permeability, the parameter we are trying to characterize. Second, the discharge rates show the best correlation with the lake areas with a quasi-linear relation between the log-transformed data (see Figure 5a). Then the discharge rate normalized by the lake area includes the least bias generated by the different geometrical settings for the lakes we compared and allows for a comparison of lakes with different areas.

4.3. Sensitivity Analysis

The sensitivity of the steady state model to input parameters (lake area and depth, evaporation, precipitation and gas exchange rate, and the chloride concentration and radon activity in the lake, the surface water inflow, the groundwater inflow, and the precipitation) is represented in Figure 6. The discharge rate calculated for a typical lake, defined as a lake which parameters equal the average value of all lakes (see Table 1), is represented while varying continuously the 12 parameters sequentially from 50 to 150% of their measured mean or assumed value. The two first graphs, which represent the changes in discharge rate while varying the chloride concentration in lake and in surface inflow, show unexpected patterns as the model actually diverges for a certain range of values. The divergence occurs when the difference between inflow and lake chloride concentration tends to zero. The calculation of the discharge rate in our model is based on the difference between the chemical activities in surface inflow and in the lakes. Therefore, the estimation of the discharge rate is biased for a range of values for $C_{S,Cl}$ and C_{Cl}, when their difference is too small to enable the differentiation between water from the surface inflow from the lake water. In this case, chloride would not make a relevant tracer, because the discharge rates are divergent. However, away from this divergence, the discharge rate is stable and not very sensitive to chloride concentrations. Then, our results are not much affected by the model instability as long as we ensure that the values of both parameters lay outside of the critical interval, i.e., a modification of one of the values by 10% leads to less than 20% change in the discharge rate.

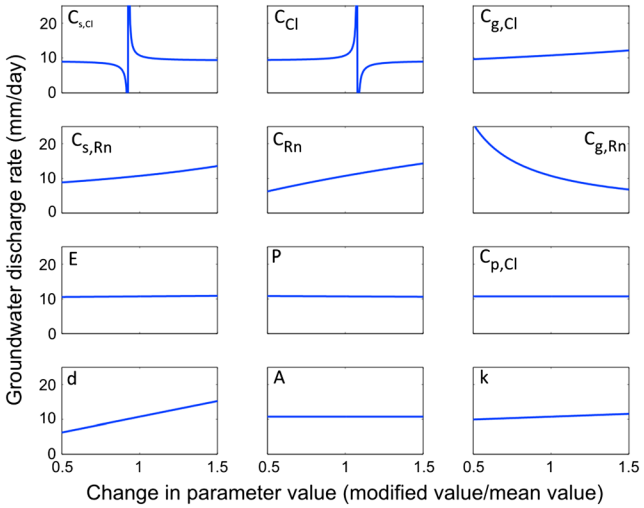

Figure 6. Sensitivity analysis to the model parameters, in order: chloride concentration in surface inflow (C_{sCl}), in lake (C_{Cl}), in groundwater (C_{gCl}), radon activity in surface inflow (C_{sRn}), in lake (C_{Rn}) and in groundwater (C_{gRn}), evaporation rate (E), precipitation rate (P), chloride concentration in precipitation (C_{pCl}), lake depth (d), lake area (A), and gas exchange rate (k). Each parameter is varied over a range of ±50%. The steady state model was applied to a typical lake with average values for dimensions and concentrations. The curve represents the variation of the calculated discharge rate while varying one of the parameters from −50% (0.5) to 50% (1.5). The steeper the slope, the more weighted is the parameter to model estimations.

Hence, the cutoff criteria are different for each lake, and lakes that do not meet that criteria were analyzed after the Monte Carlo analysis, as it is discussed further. For the other parameters, the variation is monotonic and relatively low except for the radon activity in groundwater and in the lake as well as the lake depth.

In addition, we assessed the overall sensitivity, calculating the mean discharge rates for all the lakes while varying the input parameters, and averaging the observed variations (Figure S9). Every parameter was varied sequentially by respectively ±20% and ±50% and the averages of the calculated discharge rates for the 54 lakes were plotted for each variable. The most sensitive variable is the radon activity in groundwater. A change of 50% in the radon activity in groundwater leads to a change of 120% in the averaged discharge rate, giving this parameter a crucial role that will be discussed below. The model is less sensitive to the evaporation and precipitation rates, chloride concentrations in groundwater, in precipitation, and in surface water and lake area. However, it is moderately sensitive to lake radon activity, lake depth, and the gas exchange rate. The gas exchange rate carries an important uncertainty, as it was not directly measured but rather assumed by a value computed by *Cook et al.* [2008] in small wetlands. However, since the variation with the gas exchange rate is linear, as it is shown in Figure 6a, and should be similar for all the lakes since the lakes are in a similar climate and have a similar size. A wrong estimation of the gas exchange rate will change all the results in the same way and will not affect the comparison between the lakes located on a fault zone and the others.

Because the radon activity in groundwater is a crucial parameter, the sensitivity of our model to groundwater radon activity was further investigated using a Monte Carlo method. The discharge model was run 5000 times, considering the radon activity in groundwater as a random variable, following the observed distribution, which is a lognormal distribution. The average difference between the median of the Monte Carlo simulation and the value previously estimated with the analytical model is 12%. The median discharge rates are equal to the results of the former estimations with less than 20% error for all the lakes, so that the error caused by the uncertainty in groundwater radon activity is acceptable in our study and will not change our result.

Table 1. Mean Parameter Values Used in Calculations for a Typical Lake

Parameters	Values
Area	0.8 km^2
Depth	4.9 m
Radon activity in lake	0.3 Bq/L
Radon activity in inflow	0.5 Bq/L
Radon activity in groundwater	34.5 Bq/L
Chloride concentration in lake	3.8 mg/L
Chloride concentration in surface inflow	4.6 mg/L
Chloride concentration in groundwater	13.8 mg/L

The impact of cumulative uncertainties on the discharge rates was also assessed with a Monte Carlo method. The model was run for 5000 realizations considering all the parameters as random variables following a normal distribution

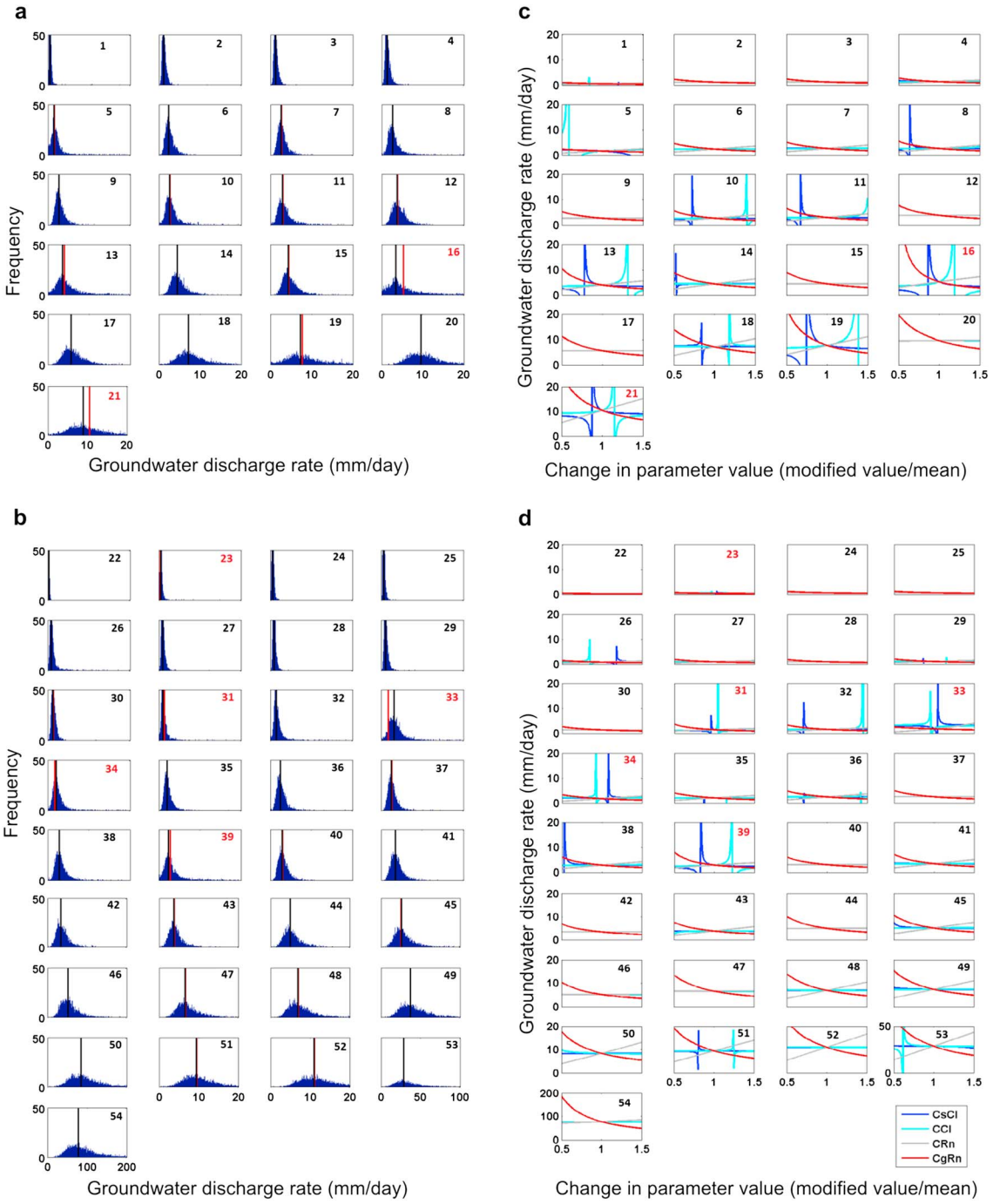

Figure 7. The results of Monte Carlo simulation for cumulative uncertainty are represented with histograms for (a) the lakes with fault and (b) the lakes without fault. The vertical black line represents the median discharge rate of Monte Carlo results, whereas the red line represents the previously estimated discharge rate. When both lines do not overlap (seven lakes with numbers in red), there is a significant difference between the estimated discharges from both methods. (c) The lakes with fault and for (d) the lakes without fault, the sensitivity of the model to four parameters (chloride concentrations and radon activities in surface inflow and in the lakes) is represented for each lake. The four parameters are varied sequentially by ±50%. When the peaks are near the middle of the graph, the measured chloride concentrations are in the critical range, and the estimations of the discharge rates from the original measures could be biased.

with a mean equal to our estimations of the parameters and a standard deviation of 20% of the mean. The histograms of the results of the Monte Carlo simulation for each lake are represented in Figures 7a and 7b. For seven lakes (numbered 16, 21, 23, 31, 33, 34, and 39), the discharge rate estimated with original values, and the median discharge rate calculated with the Monte Carlo results show more than 10% difference, suggesting that the discharge rate calculated with the measured values is less reliable. However, for the remaining 47 lakes, the differences between the mean discharge rates of the 5000 realizations and the model

Table 2. Statistics Results With Bold Indicating That the Null Hypothesis Was Rejected[a]

Number of Lakes Considered			Fault (Orogen) Versus No Fault (Orogen)	Fault (Orogen) Versus No fault (Shield)	No Fault (Orogen) Versus No Fault (Shield)
54	Welch test	*t stat*	*0.53*	**5**	**4.1**
		p value for analytical model	0.60	**2×10^{-5}**	**2×10^{-4}**
		mean *p* value from Monte Carlo	0.65	**8×10^{-9}**	**7×10^{-9}**
	KS test	*t stat*	*0.48*	**5.08**	**3.79**
		p value for analytical model	0.63	**1×10^{-5}**	**4×10^{-4}**
		mean *p* value from Monte Carlo	0.61	**2×10^{-7}**	**5×10^{-8}**
47	Welch test	*t stat*	*0.2*	**4.9**	**4.1**
		p value for analytical model	0.85	**2×10^{-5}**	**1.6×10^{-4}**
		mean *p* value from Monte Carlo	0.56	**8×10^{-9}**	**1×10^{-8}**
	KS test	*t stat*	*0.17*	**0.69**	**0.61**
		p value for analytical model	0.85	**8×10^{-5}**	**2.9×10^{-4}**
		mean *p* value from Monte Carlo	0.59	**2×10^{-7}**	**3×10^{-7}**

[a]The mean *p* value from the Monte Carlo simulations for a varying radon activity in groundwater is also indicated.

estimated discharge rate are less than 10%, and the standard deviations of the 5000 realizations are within 60% of the mean discharge rates.

Figures 7c and 7d depict the variability of the calculated discharge rates. The curves show how the discharge rate varies with chloride concentration in the lake, in the surface inflow and the radon activity in the lake and in groundwater varying from −50% to +50% of the measured value. For 16 lakes, chloride concentrations cause instability, and that situation corresponds to the lakes where chloride concentrations measured in surface inflow and in the lake are close. And for the seven above mentioned lakes, the instability occurs for values of chloride concentration corresponding to the measured values, explaining why the previously estimated value is different from the median values of the Monte Carlo results. However, the sensitivity to chloride concentrations in both water bodies is insignificant away from the critical zone, and the estimation of the discharge rate changes by less than 1% when the value of chloride concentration changes by 50%. Then, for the seven lakes that show a larger uncertainty, the estimation through Monte Carlo method is more reliable as it corresponds to noncritical values for chloride concentrations. Therefore, the discharge rates analyzed in the following statistical analysis are the median values calculated from the Monte Carlo simulation.

4.4. Statistical Analysis

We used statistical analysis to test the above qualitative assessment suggesting that there is no difference in the groundwater discharge rate for lakes located on fault and the others. We sequentially compared pairs of discharge rates from the three populations: lakes in the Appalachian orogen with fault zones, lakes in the Appalachian orogeny without fault zones, and the lakes on crystalline bedrock of the Canadian Shield. The distribution of the three data sets is lognormal (Figure S2). Therefore, we apply both the Welch *t* test and the Kolmogorov-Smirnov test [*Lilliefors*, 1967; *Marsaglia et al*., 2003; *Massey*, 1951; *Miller*, 1956] to the paired log-transformed data sets.

First, when comparing the lakes from the Appalachians overlying a fault zone and the ones from the Appalachians not overlying a fault zone, the null hypothesis stipulating that the means of both populations are the same is not rejected for both of the statistics tests (Table 2). The values of the *t* statistics, which illustrates the difference between the two groups, are low, suggesting that we cannot differentiate the groups of lakes with our data. The *p* values of both tests are high (63% and 60% for respectively the Welch *t* test and the Kolmogorov-Smirnov test), confirming that with our results, we cannot show a statistically significant difference in the groundwater discharge rates for the lakes located on a fault and the lakes not underlain a fault zone. Comparing both populations to the discharge rates calculated in the Canadian Shield with the two tests indicates that the Appalachian lakes are different than the Canadian Shield lakes with a

high significance. We also analyzed the subset of 47 lakes with lower cumulative uncertainty in the Monte Carlo simulation. The statistical results were the same with higher *p* values (Table 2). Finally, the robustness of the two statistics tests regarding the uncertainty of the radon activity in groundwater was assessed using the Monte Carlo analysis described above. We calculated both statistics tests for each run of the Monte Carlo simulation, and the mean *p* values are shown in Table 2. They are close to the original *p* values, suggesting the first estimation is correct, and the null hypothesis could not be rejected for more than 99% of the simulations, suggesting that there is no significant difference between the lakes in orogeny overlying a fault zone or the ones not underlain by a fault zone. The results of the Monte Carlo simulation were also compared to results of a similar Monte Carlo simulation applied to the lakes in the Canadian Shield. The null hypothesis was rejected for 100% of the simulations confirming that groundwater discharge rates in the Canadian Shield are different from the discharge rates in the Appalachians.

In sum, whereas the discharge rates estimated in the Appalachian region are significantly different from the discharge rates estimated in the Canadian Shield, there is no significant difference between the discharge rates of groundwater to lakes underlying faults and to lakes that do not underlie fault in the Appalachian region. One reason for the lack of effects of faults on groundwater discharge may be that the additional groundwater that is captured by a vertical fault is too small to detect. Lakes with or without faults both capture local groundwater flow. Groundwater discharge to a lake depends on the local hydraulic gradient and permeability as well as the discharge of regional groundwater systems. The extent of regional flow that bypasses local discharge zones such as lakes depends strongly on the dimensions of the watershed and the aquifer, the local relief as well as the ratio of recharge to hydraulic conductivity [*Tóth*, 1963; *Winter*, 1978]. The study areas consist of small watersheds with a humid climate, gentle relief, and generally low permeability suggesting the water table is topographically controlled [*Haitjema and Mitchell-Bruker*, 2005]. In topography-controlled water table conditions, regional flow rates are a lower percentage of total groundwater flow [*Gleeson and Manning*, 2008; *Gleeson et al*., 2011], making the perturbation of regional groundwater flow by faults difficult to observe. Another reason for the lesser effect of fault zones on groundwater discharge may be that the permeability of these old faults has evolved over time to closely mimic the surrounding rocks due to cementation. Fault deformation occurred before, during, and after the Ordovician Taconian orogeny, during the Late Silurian to early Devonian and during the Devonian Acadian orogeny [*Sasseville et al*., 2008; *Séjourné and Malo*, 2007]. Some of the fault deformation is of similar age to the deformed lithologies. A final reason for the limited effect of fault zones on groundwater discharge may be that in such old orogen, major faults may be less significant in determining groundwater flow than the numerous smaller fractures, joints, and bedding planes. Interesting future research questions are whether the difference in discharge rates would be significant in (1) higher permeability region where the permeability differences may be greater and/or (2) in more tectonically active regions where the fracture networks may be less cemented.

5. Conclusions

Groundwater discharge rates to 54 lakes underlying sedimentary and volcanic Paleozoic rocks in eastern Québec have been estimated in order to assess the impact of fault zones on groundwater discharge. The model used to quantify the groundwater discharge rates combines radon and chloride mass balances and includes radon and chloride contribution from groundwater and surface water inflow, as well as chloride contribution from precipitation and radon loss through radioactive decay and gas exchange. We draw two main conclusions. First, discharge rates estimated in the Canadian Shield are significantly lower than the discharge rates estimated in the Appalachian region. This suggests that this method may be a useful proxy for permeability, since the crystalline rocks in the Canadian Shield have significantly lower permeability than sedimentary and volcanic rocks in the Appalachian. Second, there is no significant difference between the groundwater discharge rates in areas overlying fault zones and in areas without fault zone in this old orogen. Hence, although fault zones change the local permeability, shallow fault zones may have no significant impact on the regional groundwater discharge in tectonically inactive orogen. It is uncertain whether these faults are barriers, conduits, or combined conduit-barriers.

These results may have implications for other inactive fault zones as well as providing a new methodology for examining fluid flow around fault zones. The quantification of groundwater flow using radon forms a potential method that can help understanding fault zones impact on regional groundwater systems in many

geological settings. Because not all the geological settings would lead to the same conclusion that fault zones do not considerably affect regional groundwater flow, we suggest that an integrative approach be used and a database of fault zones be built, classifying fault zones with their geological characteristics (type of fault, fault architecture, and surrounding bedrock) as well as geographical characteristics (watershed dimensions, topography, and lake interconnections), and referencing their impact on regional flows.

Acknowledgments
T.G. is supported by NSERC and CIFAR. We thank M. Larocque and S. Gagné from the Earth and Atmospheric Science department at UQAM for allowing us to complete the radon analysis and for helping us throughout our research. We also thank J. McKenzie and M. Baraer from the Earth and Planetary Sciences department at McGill for enabling us to carry out the ions analysis and for their kind help and advice. Acknowledgments also go to S. Gaskin from McGill University and all members of our research group for providing suggestions on earlier versions of this manuscript. Two anonymous reviewers significantly improved this manuscript.

References

Aydin, A. (2000), Fractures, faults, and hydrocarbon entrapment, migration and flow, *Mar. Pet. Geol.*, *17*, 797–814.
Bense, V. F., and M. A. Person (2006), Faults as conduit-barrier systems to fluid flow in siliciclastic sedimentary aquifers, *Water Resour. Res.*, *42*, W05421, doi:10.1029/2005WR004480.
Bense, V. F., M. A. Person, K. Chaudhary, Y. You, N. Cremer, and S. Simon (2008), Thermal anomalies indicate preferential flow along faults in unconsolidated sedimentary aquifers, *Geophys. Res. Lett.*, *35*, L24406, doi:10.1029/2008GL036017.
Bense, V. F., T. Gleeson, S. E. Loveless, O. Bour, and J. Scibek (2013), Fault zone hydrogeology, *Earth Sci. Rev.*, *127*, 171–192, doi:10.1016/j.earscirev.2013.09.008.
Caine, J. S., J. P. Evans, and C. B. Forster (1996), Fault zone architecture and permeability structure, *Geology*, *24*, 1025–1028.
Chester, F. M., and J. M. Logan (1986), Implications for mechanical properties of brittle faults from observations of the Punchbowl Fault Zone, California, *Pure Appl. Geophys.*, *124*, 80–106.
Childs, C., T. Manzocchi, J. J. Walsh, C. G. Bonson, A. Nicol, and M. P. J. Schöpfer (2009), A geometric model of fault zone and fault rock thickness variations, *J. Struct. Geol.*, *31*, 117–127.
Cook, P. G. (2003), *A Guide to Regional Groundwater Flow in Fractured Rock Aquifers*, CSIRO Land and Water, Henley Beach, AU.
Cook, P. G., S. Lamontague, D. Berhane, and J. F. Clark (2006), Quantifying groundwater discharge to Cockburn River, Southeastern Australia, using dissolved gas tracers ^{222}Rn and SF^{6}, *Water Resour. Res.*, *42*, W10411, doi:10.1029/2006WR004921.
Cook, P. G., C. Wood, T. White, C. T. Simmons, T. Fass, and P. Brunner (2008), Groundwater inflow to a shallow, poorly-mixed wetland estimated from a mass balance of radon, *J. Hydrol.*, *354*, 213–226.
De Souza, S., and A. Tremblay (2010), The Rivière-des-Plante ultramafi c Complex, southern Québec: Stratigraphy, structure, and implications for the Chain Lakes massif, in *From Rodinia to Pangea—The Lithotectonic Record of the Appalachian Region: Geological Society of America Memoir*, vol. 206, edited by R. P. Tollo et al., pp. 1–17, Geological Society of America, Boulder, Colo.
Dimova, N. T., W. C. Burnett, J. P. Chanton, and J. E. Corbett (2013), Application of radon-222 to investigate groundwater discharge into small shallow lakes, *J. Hydrol.*, *486*, 112–122.
DMTI (2010), CanMap Water.
Evans, J. P., C. B. Forster, and J. V. Goddard (1997), Permeability of fault-related rocks, and the implications for hydraulic structure of fault zones, *J. Struct. Geol.*, *19*, 1393–1404.
Fairley, J. P., and J. J. Hinds (2004), Rapid transport pathways for geothermal fluids in an active Great Basin fault zone, *Geology*, *32*, 825–828.
Fairley, J. P., J. Heffner, and J. J. Hinds (2003), Geostatistical evaluation of permeability in an active fault zone, *Geophys. Res. Lett.*, *30*(18), 1962, doi:10.1029/2003GL018064.
Faulkner, D. R., C. A. L. Jackson, R. J. Lunn, R. W. Schlische, Z. K. Shipton, C. A. J. Wibberley, and M. O. Withjack (2010), A review of recent developments concerning the structure, mechanics and fluid flow properties of fault zones, *J. Struct. Geol.*, *32*, 1557–1575.
Folger, P. F., E. P. Poeter, R. B. Wanty, D. Frishman, and W. Day (1996), Controls on ^{222}Rn variations in a fractured crystalline rock aquifer evaluated using aquifer tests and geophysical logging, *Ground Water*, *34*, 250–261.
Gleeson, T. (2009), Groundwater recharge, flow and discharge in a large crystalline watershed, Department of Civil Engineering Published, PhD thesis, 251pp., Queen's University, Kingston, Ontario.
Gleeson, T., and A. H. Manning (2008), Regional groundwater flow in mountainous terrain: Three-dimensional simulations of topographic and hydrogeologic controls, *Water Resour. Res.*, *44*, W10403, doi:10.1029/2008WR006848.
Gleeson, T., K. Novakowski, P. G. Cook, and T. K. Kyser (2009), Constraining groundwater discharge in a large watershed: Integrated isotopic, hydraulic, and thermal data from the Canadian Shield, *Water Resour. Res.*, *45*, W08402, doi:10.1029/2008WR007622.
Gleeson, T., L. Marklund, L. Smith, and A. H. Manning (2011), Classifying the water table at regional to continental scales, *Geophys. Res. Lett.*, *38*, L05401, doi:10.1029/2010GL046427.
Haitjema, H. M., and S. Mitchell-Bruker (2005), Are water tables a subdued replica of the topography?, *Ground Water*, *43*, 781–786.
Hayashi, M., and D. O. Rosenberry (2002), Effects of ground water exchange on the hydrology and ecology of surface water, *Ground Water*, *40*, 309–316.
Kalbus, E., F. Reinstorf, and M. Schirmer (2006), Measuring methods for groundwater-surface water interactions: A review, *Hydrol. Earth Syst. Sci.*, *10*, 873–887.
Kiro, Y., Y. Yechieli, C. I. Voss, A. Starinsky, and Y. Weinstein (2012), Modeling radium distribution in coastal aquifers during sea level changes: The Dead Sea case, *Geochim. Cosmochim. Acta*, *88*, 237–254.
Kluge, T., J. Ilmberger, C. von Rohden, and W. Aeschbach-Hertig (2007), Tracing and quantifying groundwater inflow into lakes using a simple method for radon-222 analysis, *Hydrol. Earth Syst. Sci.*, *11*, 1621–1631.
Kluge, T., C. von Rohden, P. Sonntag, S. Lorenz, M. Wieser, W. Aeschbach-Hertig, and J. Ilmberger (2012), Localising and quantifying groundwater inflow into lakes using high-precision ^{222}Rn profiles, *J. Hydrol.*, *450–451*, 70–81.
Leray, S., J. R. de Dreuzy, O. Bour, T. Labasque, and L. Aquilina (2012), Contribution of age data to the characterization of complex aquifers, *J. Hydrol.*, *464–465*, 54–68.
Leray, S., J. R. de Dreuzy, O. Bour, and E. Bresciani (2013), Numerical modeling of the productivity of vertical to shallowly dipping fractured zones in crystalline rocks, *J. Hydrol.*, *481*, 64–75.
Lilliefors, H. W. (1967), On the Kolmogorov-Smirnov test for normality with mean and variance unknown, *J. Am. Stat. Assoc.*, *62*, 399–402.
Marsaglia, G., W. Tsang, and J. Wang (2003), Evaluating Kolmogorov's distribution, *J. Stast. Software*, *8*, 1–4.
Massey, F. J. (1951), The Kolmogorov-Smirnov test for goodness of fit, *J. Am. Stat. Assoc.*, *46*, 68–78.
Miller, L. H. (1956), Table of percentage points of Kolmogorov statistics, *J. Am. Stat. Assoc.*, *51*, 111–121.
Oxtobee, J. P. A., and K. S. Novakowski (2002), A field investigation of groundwater/surface water interaction in a fractured bedrock environment, *J. Hydrol.*, *269*, 169–193.

Praamsma, T. W., K. S. Novakowski, T. K. Kyser, and K. Hall (2009), Using stable isotope and hydraulic head data to investigate groundwater recharge and discharge in a fractured rock aquifer, *J. Hydrol.*, *366*, 35–45.
Prairie, Y., and A. Soucisse (1999), Rapport sur le suivi de la qualité des eaux, RAPPEL.
Sasseville, C., A. Tremblay, N. Clauer, and N. Liewig (2008), K–Ar age constraints on the evolution of polydeformed fold–thrust belts: The case of the Northern Appalachians (southern Quebec), *J. Geodyn.*, *45*, 99–119.
Schoonmaker, A., and W. S. F. Kidd (2007), A reappraisal of the allochthonous nature of the Rosenberg slice and Stanbridge Group of southern Quebec and northwestern Vermont, *Can. J. Earth Sci.*, *44*, 155–169.
Schroetter, J.-M., J. H. Bédard, and A. Tremblay (2005), Structural evolution of the Thetford Mines Ophiolite Complex, Canada: Implications for the southern Québec ophiolitic belt, *Tectonics*, *24*, TC1001, doi:10.1029/2003TC001601.
Schroetter, J.-M., A. Tremblay, J. H. Bédard, and M. E. Villeneuve (2006), Syncollisional basin development in the Appalachian orogen—The Saint-Daniel Mélange, southern Québec, Canada, *Geol. Soc. Am. Bull.*, *118*, 109–125.
Seaton, W. J., and T. J. Burbey (2005), Influence of ancient thrust faults on the hydrogeology of the Blue Ridge province, *Ground Water*, *43*, 301–313.
Séjourné, S., and M. Malo (2007), Pre-, syn-, and post-imbrication deformation of carbonate slices along the southern Quebec Appalachian front—Implications for hydrocarbon exploration, *Can. J. Earth Sci.*, *44*, 543–564.
Séjourné, S., J. Dietrich, and M. Malo (2003), Seismic characterization of the structural front of southern Quebec Appalachians, *Bull. Can. Pet. Geol.*, *51*, 29–44.
Séjourné, S., M. Malo, M. M. Savard, and D. Kirkwood (2005), Multiple origin and regional significance of bedding parallel veins in a fold and thrust belt: The example of a carbonate slice along the Appalachian structural front, *Tectonophysics*, *407*, 189–209.
Sophocleous, M. (2002), Interactions between groundwater and surface water: The state of the science, *Hydrogeol. J.*, *10*, 52–67.
St-Julien, P., and A. Slivitzsky (1985), Compilation géologique de la région de l'Estrie-Beauce, Rapport MM 85–04, Gouvernement du Québec, Ministère de l'Énergie et des Ressources.
Taniguchi, M., W. C. Burnett, J. E. Cable, and J. V. Turner (2002), Investigation of submarine groundwater discharge, *Hydrol. Processes*, *16*, 2115–2129.
Tóth, J. (1963), A theoretical analysis of groundwater flow in small drainage basins, *J. Geophys. Res.*, *68*, 4795–4812.
Williams, H. (1979), Appalachian orogen in Canada, *Can. J. Earth Sci.*, *16*, 792–807.
Winter, T. C. (1978), Numerical simulation of steady-state three-dimensional groundwater flow near lakes, *Water Resour. Res.*, *14*, 245–254.
Winter, T. C. (1999), Relation of streams, lakes, and wetlands to groundwater flow systems, *Hydrogeol. J.*, *7*, 28–45.
Winter, T. C., J. W. Harvey, O. L. Franke, and W. M. Alley (1998), Ground water and surface water: A single resource, *U.S. Geol. Surv. Circ.*, *1139*, 79.